Shock processing of materials with laser initiated spherically convergent detonations

Frederick J. Mayer, Walter B. Fechner, Robert L. Maynard, Nancy W. Schmerberg, and Michael R. Wixom
KMS Fusion, Incorporated, P.O. Box 1567, Ann Arbor, Michigan 48106

(Received 12 February 1988; accepted for publication 17 June 1988)

We describe a new technique for dynamically compressing materials using small scale spherically converging shock waves driven by laser initiated high explosives. This technique uses spherical targets consisting of an outer explosive shell of 1–2 cm diam, and an inner sample core 0.48–0.96 cm diam. The shock waves result from a detonation wave generated near the outer surface of the explosive by a high-power laser. Spherical convergence and shock impedance matching produce ingoing shock waves in the core which have pressure amplitudes much greater than the detonation pressure of the explosive. Shock pressures in the sample core are typically in the range 10–200 GPa depending on the radius, density, and composition of both the explosive layer and the inner core. We discuss the hydrodynamic modeling of our implosion process, the conditions required for laser initiated detonation, and the results of boron nitride and carbon recovery experiments.

I. INTRODUCTION

Dynamic high-pressure research is motivated in part by the potential use of shock waves in solid materials to induce desirable changes such as polymorphic phase transitions or powder consolidation. The most familiar examples include the graphite to diamond phase transition[1] and the graphitic boron nitride (gBN) to wurtzite boron nitride phase (wBN) transition.[2] These phase transitions occur at shock pressures in excess of 23 GPa[3] and 10 GPa,[4] respectively. The production of diamond[5–7] and wBN[8,9] is the first successful commercial application of shock wave processing. We have developed a new shock processing technique which is easy to handle on a small scale yet lends itself to high repetition rates desirable in commercial processing applications. Our technique uses laser initiated spherically convergent detonations to shock process centrally located cores of sample material.[10] The laser provides a convenient means of producing a spherically convergent detonation without the use of explosive lenses. The benefits of spherical geometry include pressure amplification with convergence and absence of center of mass target velocity. With further gains in high-power laser technology, spherical shock processing without explosives may become feasible.

II. IMPLOSION DYNAMICS AND THEORETICAL MODELING

A distinct advantage of shock processing in spherical geometry is the simplicity of the hydrodynamic modeling. Computer simulations of the implosion process are performed with a one-dimensional Lagrangian hydrocode referred to as CHICODE. CHICODE was developed at KMS to assist in target design for spherical shock processing experiments.

The cross section of a typical target is shown in Fig. 1. The centrally located payload is typically 0.48–0.96 cm in diameter. Since many of the samples to be processed are weak or brittle, the payloads often include a steel or aluminum shell to eliminate contamination and recovery problems associated with fragmentation.

CHICODE is used to optimize pressure, temperature, and "confinement time" which we define as the time from which the outer sample mesh zone exceeds a specified pressure, e.g., 20 GPa, until the central sample mesh zone drops below this specified pressure. This optimization procedure generally amounts to selecting among a short list of sample and container materials and varying the thicknesses of the explosive and container layers to maximize either peak pressure or confinement time.

CHICODE specifics are as follows: Steady-state detonations are modeled with the Jones, Wilkins, and Lee (JWL) equation of state (EOS).[11] For our purposes, the most important feature of the explosive EOS is the ability to allow for spherical convergence effects. The JWL EOS is a suitable choice in this regard.

For sample and container materials, the EOS are taken from the SESAME EOS tables.[12] The CHICODE calculations do not self-consistently include the actual phase transition in

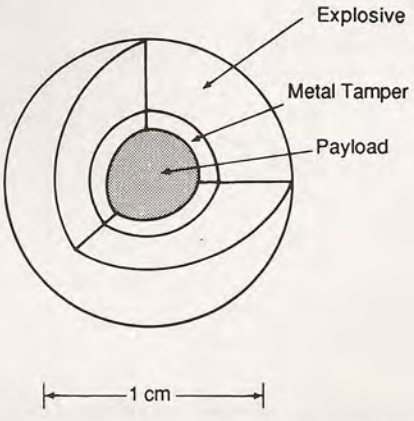

FIG. 1. Design of typical target for shock processing materials by spherically convergent detonations.

 0021-8979/88/224896-07$02.40

the EOS of the shocked material. In other words, the shocked graphite is treated as high density graphite rather than as diamond. The reason for this approach was the lack of a suitable algorithm for treating the phase transition. One of us (W.B.F.) has developed an appropriate algorithm for convergent shock waves in materials undergoing a phase transition which will be discussed in a future publication. Materials strengths are included in CHICODE in the manner suggested by Mader.[13] Shear moduli and yield strengths are taken from the Physics Vade Mecum and implemented in the manner described in Mader (pp. 310–332). Heat conduction is done with standard diffusive algorithms using thermal conductivities taken from several standard references.

CHICODE can also accommodate material heterogeneities in the form of porosity or alloys. Porous materials are simply heated as uniform underdense materials with a density equaling the mass divided by the total volume of samples and pores. Material strengths are ignored. This algorithm forces the porous material to do work equal to $\frac{1}{2}P\Delta V$ to get to a nonporous density where P is the shock pressure and ΔV is the difference in volume between the porous and nonporous material. Alloys and heterogeneous mixtures are handled in the "V-E" manner described by Hsu *et al.*[14]

A key to our materials processing technique is the increase in shock pressure and temperature which occurs with spherical convergence of the shock wave. The convergence effects as calculated by CHICODE are illustrated in Fig. 2. In this example the core consists of fully dense graphite surrounded by an aluminum container. The explosive is PETN at a density of 1.0 g/cm^3. The steady-state detonation pressure (without spherical convergence) for PETN at this density is 8.7 GPa. The shock enters the graphite core with a calculated pressure of about 25 GPa. In this particular example, the pressure increase from 8 to 25 GPa is the combined result of both spherical convergence and shock impedance matching between the explosive and the payload. Convergence amplifies the pressure of the inward propagating shock with an apparent scaling factor of $r^{-0.7}$. Central reflection of the shock wave generates a return shock with an additional pressure gain of 1.5–2.0 over the pressure of the initial shock.

When modeling the convergence of the shock waves, we have tacitly assumed that no significant attenuation occurs and that the converging shocks are stable. We neglect attenuation in our small targets ($r < 0.5$ cm) since it is expected to become evident only at larger scales.[15–17] Stability is here defined as the tendency for asymmetries in the imploding shock front to washout, thus maintaining a spherical shock front. Invalidity of the stable shock front assumption could produce substantial discrepancy between the actual and the calculated pressures. We are aware of only the experiments by Perry and Kantrowitz[18] to verify the stability of converging shock waves, and their results are for cylindrical rather than spherical geometry. Since some of our targets are designed to produce phase transitions in the innermost 2–3 mm of a 2-cm target, our actual peak pressures could be well short of the calculated peak pressures if stability and symmetry are not maintained.

Figure 3 shows a typical pressure history as calculated by CHICODE for an outer zone of the sample core. Since, in spherical geometry, the bulk of the material is located in the outer shell, this pressure profile is representative of the conditions under which most of the sample is processed. The sharp peak late in time corresponds to the passage of the outbound reflected shock through sample material having an inbound particle velocity. CHICODE can be used to determine how well the reflected shock zeros out the particle velocity and limits the fragmentation of the core. For such an effect to occur, the impedance match between the sample and tamper must be close to avoid strong reflections or rarefactions. In theory, CHICODE can also help design a multilayer target with quasi-isentropic core heating via multiple reflection (ring-up). Unfortunately, the simulations indicated that multiple reflections were difficult to achieve (especially in the outward bound phase) and even then only yield small pressure increases.

The small scale and spherical geometry result in significantly different implosion dynamics for our samples compared to the dynamics for other shock recovery fixtures used in BN and diamond synthesis. These other fixtures generally

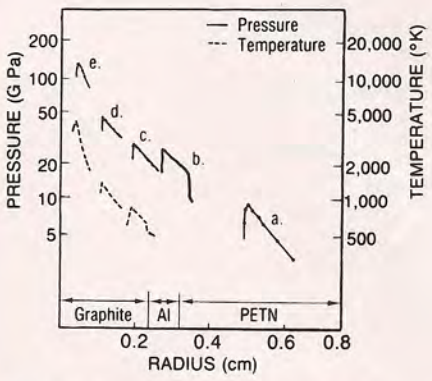

FIG. 2. Radial temperature and pressures calculated by CHICODE at times $a = 0.6$, $b = 0.9$, $c = 1.0$, $d = 1.10$, and $e = 1.15$ μs. The initial densities of the target components were 1.0 g/cm^3 for PETN, 2.7 g/cm^3 for aluminum, and 2.25 g/cm^3 for graphite.

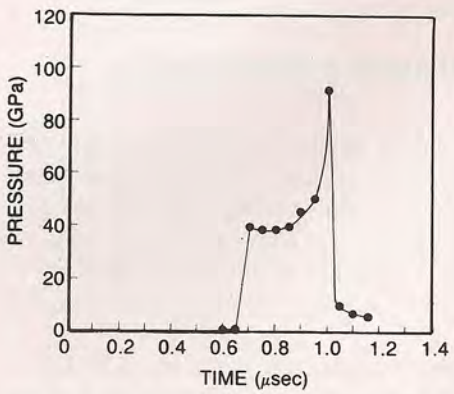

FIG. 3. Pressure history in zone near outer edge of a 60% dense diamond core with 2.4-mm radius. The core was surrounded by a 0.3-mm-thick aluminum tamper and a 4.0-mm-thick layer of PETN at 1.5 g/cm^3.

fall into either of two classes. Most experimental fixtures use a planar flyer or detonation wave to shock a disk of sample material mounted in a much larger metal container. The sample dimensions are typically 1–2 cm thick and 5–10 cm diam. Although the initial shock can be quite planar, the container geometry produces a strong axial reflection and complicated edge effects.[16,17] Relative to our spherical target design, these pseudoplanar fixtures tend to produce longer confinement times and more nonuniform conditions.

The second common configuration for shock processing materials is the "cylindrical zipper" arrangement. In this configuration, an outer cylinder of explosive drives an inner cylindrical metallic flyer plate onto a sample tube. The axial propagation of the detonation wave down the explosive cylinder zips the flyer plate along the sample tube. This geometry[5–9] is used for commercial production of shock formed diamond and wBN. The sample tube dimensions are approximately 10 cm in diameter and up to a meter or more in length. These recovery fixtures can be designed to provide reasonably uniform conditions since the axial detonation does not produce a strong radially convergent component. The confinement times achieved in these large fixtures are much longer than in our spherical assemblies.

III. LASER INITIATION OF DETONATION

The high explosive ignition requirements are an important issue in implementing our technique. There have been a number of studies on laser ignition of high explosives, most using 25-ns ruby laser pulses or 100-ns Nd-glass laser pulses.[19–22] The typical short pulse ignition energy flux has been found to be 1–5 J/cm^2. This value is not unexpected as it is about equal to observed optical material damage levels.

It was necessary for several reasons to reproduce and extend these results. Since our laser energy was limited to 100 J, an ignition threshold of 5 J/cm^2 placed an upper limit on target size of 2.5 cm diam. Given that the sample size is some small fraction of the target diameter, any practical applications would require the lowest possible threshold. For the same reason, it was also necessary to establish that laser initiated detonations do not require a large run-up distance. Finally, it was important to address the uniformity of the laser initiation. If ignition near the threshold was at widely separated hot spots the benefits of spherical symmetry would not be realized.

Several explosives were considered for our shock processing technique, including 2,4,6-trinitro-1,3,5-benzenetriame (TATB), octahydro-1,3,5,7-tetranitro-1,3,5,7-tetrazocine (HMX), and 2,2-bis[(nitroxy) methyl]-1,3-propanediol, dinitrate (PETN). TATB and HMX were tested as consolidated pellets which failed to initiate at laser energies in excess of 20 J/cm^2. The PETN initiation threshold was found to be very sensitive to porosity. Consolidated forms of PETN, especially those in which binders were used, had unacceptably high thresholds. The threshold for powdered PETN at several densities is reported in Table I. These results clearly show a sharp rise in the threshold with a drop in porosity. Our results are in good agreement with other reported values[20] for the initiation threshold even though we are irradiating a much larger surface area and are using a somewhat longer pulse.

TABLE I. Energy thresholds for laser initiated detonations.

Explosive density (g/cm^3)	Laser energy threshold (J/cm^2)
0.45	4.5
0.90	6.5
1.15	7.5

The assembly shown in Fig. 4(a) was used to determine the threshold, velocity, and run-up distance for laser initiated detonations. The detonation arrival times were detected by KMSF shock-sensor optical pins[23] embedded along the length of the explosive. Figure 4(b) shows the results of several measurements on PETN at 1.0 g/cm^3. The data indicate that the laser initiated detonations are well behaved. The inverse slope of the plotted line gives an observed value for the detonation velocity of 5.2 mm/μs for PETN at 1.0

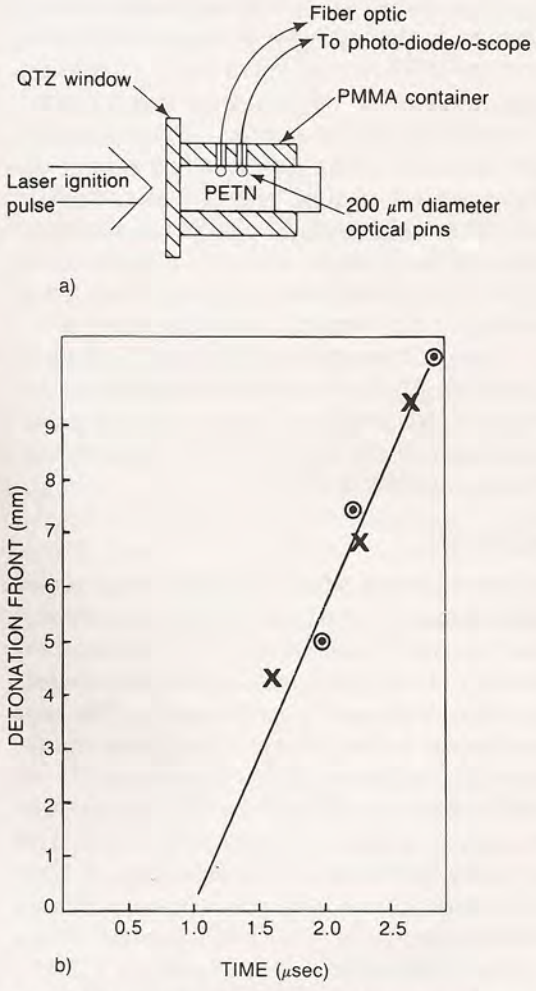

FIG. 4. (a) Experimental assembly for determining laser energy threshold and detonation arrival time. (b) Detonation velocity data for laser initiated PETN of density 1.0 g/cm^3. The two sets of data points from different shots demonstrate the reproducibility of laser initiated detonations.

g/cm^3. This observed velocity is very reproducible and in excellent agreement with the theoretical steady-state detonation velocity of 5.6 mm/μs for PETN at 1.0 g/cm^3. Similar experiments in which the pins are placed much closer to the window have demonstrated that the steady-state velocity is attained within distances of less than a millimeter of the window.

The zero time for the abscissa in Fig. 4(b) refers to the arrival of light at the target surface. The 1-μs delay before onset of detonation was observed in all experiments. This delay time is indicative of a thermal initiation mechanism as opposed to a laser driven shock process. Several other observations further confirm the thermal mechanism. For pulses in the 100 ps–100 ns range, the threshold was dependent on energy per unit area rather than power per unit area. The addition of a small percentage of micron aluminum powder reduced the threshold by a factor of 2 by increasing the absorbance and heating in the outer layer of the explosive. Coating the window with thin Al films did not lower the threshold as might be expected for a laser driven shock process. These results indicate that a buildup to thermal runaway is occurring during the delay time.

The final objective of the laser initiation experiments was to verify that targets could be initiated with adequate spherical symmetry. The first successful test was the detection of the increase in detonation velocity associated with spherical convergence. The second indication of good detonation symmetry was the observation of spherically symmetric voids at the center of solid metal cores. These voids were formed by tensile forces arising during the passage of the reflected shock wave propagating outward from the core center. The most convincing evidence of spherical symmetry is the appearance of the boron nitride core shown in Fig. 5. The central gray region is associated with the formation of wBN. This region is quite spherical with the exception of the rays which correspond to seams in the explosive hemishells and plastic container. The radius of the gray zone coincides with the point at which hydrodynamic computer code calculations predict the spherically converging shock pressure exceeds the BN transition threshold.

IV. APPARATUS

In the KMS shock processing technique a high-power laser must instantaneously satisfy a detonation threshold requirement over the entire outer surface of the spherical explosive. Uniformity of the illumination is critical to efficiently obtaining a spherically convergent detonation. The laser illumination scheme is derived from early configurations for laser driven inertial confinement fusion experiments.[24]

The optical system is built around a 100-J Nd-glass laser. The laser consists of an electro-optically Q-switched oscillator followed by four stages of rod amplifiers. A beam splitter is used to produce two equal power beams which are directed toward opposite poles of the spherical target. With a Q-switched pulse of 100 ns the total laser power is 1 GW.

Each of the two legs of the laser beam are expanded from the 80 mm diam of the final amplifier stage to a nominal 200 mm diam at the focusing lenses. The focusing optics consist of plastic Fresnel lenses with a 6-in. focal length. This configuration illuminates the target with two beams at $f/0.75$. The overlap of the two beams on the target surface produces very nearly uniform intensity. There were no signs of ignition nonuniformities due to the beam intensity variations caused by the groove pattern in the lenses.

FIG. 5. Cross section of recovered boron nitride core shock processed in PETN at 1.0 g/cm^3. The dark outer ring is the aluminum tamper, the light inner ring is untransformed boron nitride, and the central gray region is associated with transformed boron nitride.

Explosive targets are shock processed inside a detonation chamber cut from 10-in.-diam aluminum tubing. Polycarbonate windows are mounted on each face of the cylindrical chamber to transmit the laser light yet confine the target debris. A vacuum pump is connected to the chamber to reduce noise and target contamination. The chamber is equipped with several ports used for diagnostics and target mounting hardware. The target is suspended inside the chamber on a thin steel rod. The rod is held in a ball and socket vacuum feedthrough to permit rapid optical alignment by positioning the target at the fixed focal point. Optical alignment is facilitated by injecting a cw YAG laser beam down the axis of the high-power pulsed laser.

A number of diagnostics can be employed to monitor the implosion process. The shock wave time-of-arrival sensors[23] are placed in the explosive charge to measure detonation arrival times. Given the arrival time data along with the explosive density, the detonation velocity and pressure can easily be calculated. Photographic techniques are also employed as diagnostics. A simple but effective approach is open shutter visible light photography of the target. Under intense laser illumination the target surface becomes hot enough to be a blackbody emitter. The emitted light is isolated by using filters to exclude reflected laser light. The strong T^4 dependence of emission intensity makes open shutter photography a useful probe of the uniformity of target surface heating. An STL 26B framing camera is also available to provide photographs with submicrosecond time resolution.

A variety of target designs have been developed with the guidance of the hydrodynamic computer simulation code. In general these targets incorporate most or all of the following components. Spherical samples are either machined from rod stock or pressed from powders in a greenform press.

Most samples are surrounded by a metal tamping layer which serves a number of functions. This tamper plays a key role in reducing target fragmentation and is vital to the successful recovery of intact payloads containing brittle samples. The highest recovery rates are realized when the shock impedance of the tamper is only slightly greater than that of the sample, e.g., aluminum tampers and graphite cores. The tampers also prevent contamination or oxidation of the sample. Welded seams, threaded plugs, and electroplating have all been used to seal the tamper.

The tamped sample is placed between two hemishells of pressed explosive. The diameter and density of this explosive are the primary variables controlling the shock processing conditions. Because the laser initiation threshold for nonporous explosives is too high, the pressed hemishells must be surrounded by a low density powdered initiating layer. This layer is formed by dusting the inside of a transparent hemishell with a 1% mixture of 1-μm aluminum powder in ultrafine PETN. Besides lending physical support for the initiating layers, the transparent hemishells also provide a degree of confinement which lowers the detonation threshold by a factor of 2 compared to unconfined PETN powder. The transparent hemishells are generally fabricated from thermoformed PMMA sheet, although thicker cast glass hemishells were used for a small number of targets. The thick glass aided the recovery of intact targets, but the large amount of debris was troublesome. Target assembly is completed by joining the transparent hemishells with epoxy along the seam, taking care to maintain a uniform initiating layer and avoiding dead volume in the target.

V. BORON NITRIDE AND CARBON RECOVERY EXPERIMENTS

When subjected to high dynamic pressures, both carbon and boron nitride can be recovered in metastable phases. These allotropic phase transitions of graphite to diamond and graphitelike boron nitride (gBN) to wurtzite boron nitride (wBN) were selected as proof-of-principle experiments to demonstrate the feasibility of small scale spherical dynamic processing. Experiments on pure graphite[3] and gBN[4] have shown that these phase transitions are complete at shock pressures of 35 and 16 GPa, respectively. However, regraphitization driven by the residual heat from the shock process diminishes the yield of the metastable products. Recent reports suggest that the residual temperatures should be in the range of 1400–2000 K for carbon[25] and in the range of 500–2000 K for boron nitride.[26] The proof-of-principle experiments were designed to produce pressures in excess of the minima for complete transition while limiting the release temperatures to the given ranges.

Recovered payloads were analyzed by powder x-ray diffractometry to quantitatively measure the yields of wBN and diamond. Sample preparation consisted of using mineral acids to dissolve away metallic tamper or core materials followed by drying and crushing up the recovered sample. Several enhancement procedures were used including alkali fusion to isolate wBN from gBN, as well as lead oxide roasting[27] or boiling $HClO_4$ to isolate diamond from graphite and amorphous carbon.

The wBN phase was recovered from several different types of targets subjected to a wide range of shock pressures and temperatures. Successful target designs included untamped pure hot-pressed gBN, aluminum tamped pure hot-pressed gBN, and aluminum tamped copper-gBN green-formed composites. Shock pressures were varied primarily by varying the density of the PETN explosive. The detonation pressures ranged from 8.7 GPa at a density of 1.0 g/cm^3 to 30 GPa at 1.7 g/cm^3. Shock temperatures and release temperatures were adjusted by changing the payload porosity and by altering the amount and density of the powdered metal which was mixed with the gBN. When used in sufficiently large volume fractions, the high density, high shock impedance metal additives help limit the temperatures in the gBN by reducing the pressure of the initial shock in the gBN and by conducting heat away from the shock heated BN.

Over the entire pressure range the relative yield of wBN [wBN/(wBN + gBN)] from copper-gBN payloads was higher than from pure gBN payloads. Figure 6 shows the relative yield of wBN plotted as a function of detonation pressure for three types of targets. The maximum relative yield was 65% wBN recovered from a 20-wt. % gBN/Cu payload shocked by 1.5-g/cm^3 PETN. The yield from gBN/Cu targets began to drop significantly at higher shock pressures. This seems to be an indication of regraphitization of the wBN being driven by excessive heating at high shock pressures.

The relative wBN yields from both tamped and untamped pure BN were lower. The yields from both of these target designs also peaked at a detonation pressure of about 20 GPa, but the maxima are much weaker than for the gBN/Cu targets. Curiously, the absolute yields of wBN (the product of relative yield times the amount of gBN starting material) were roughly constant despite large variations in the volume of gBN due to the volume occupied by metal tampers or metal powder additives.

The diminished yields from untamped targets seem to be associated with fragmentation of the payload. For tamped targets the yield from payloads which fragmented was approximately half that from identically processed payloads which were recovered intact. The diminished yield associated with fragmentation is possibly due to enhanced regraphitization rates resulting from the large increases in surface area associated with fragmentation during the release phase.

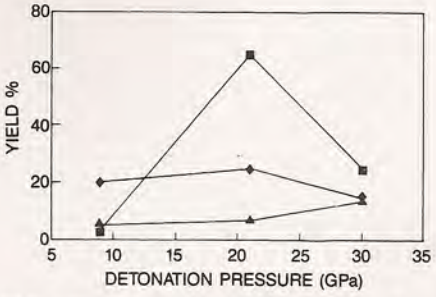

FIG. 6. Percent yield of wurtzite phase boron nitride as a function of steady-state detonation pressure. (■ tamped copper/boron nitride payload; ◆ tamped pure boron nitride payload; ▲ untamped pure boron nitride payload.)

The wBN synthesis results reported here are consistent with results reported by others in the literature.[8,9,28–30] The yield and shock conditions agree well with those reported for both planar and cylindrical recovery experiments despite large variations in physical dimensions. For the sake of comparison Fig. 7 shows a plot of yield versus shock pressure from a number of different reports. The KMS data points are connected by lines as seen in Fig. 6. In Fig. 7, the KMS copper/boron nitride points appear at higher pressure than the pure boron nitride data, showing the effect of copper in raising the shock pressure in the boron nitride.

Paradoxically, the results of our diamond recovery experiments were not consistent with much of the data reported in the literature.[6,7,25,31] Despite a large variety of starting materials, shock pressures, and target designs, none of our experiments managed to produce enough diamond to exceed our detection threshold which was estimated to be 2%. Graphite samples covered a range of densities from 0.5 to 2.2 g/cm^3 and included samples of starting materials identical to those used in both shock synthesis and static press synthesis of diamond. The payload porosity and density were varied by using a number of graphite-metal combinations including ductile cast iron, gray cast iron, hot-pressed copper graphite (nonporous), cold-pressed copper graphite (porous), and similar combinations substituting tungsten, chromium, nickel, or aluminum for the copper. Hydrocode simulations indicated that these target designs produced pressures in the 20–60-GPa range over significant volume fractions of the payload. As Fig. 8 shows, this pressure range should have been ideal for producing diamond in easily detectable quantities.

There is little doubt that our samples were reaching the calculated pressures. All of the detonation velocity and flyer velocity data demonstrate that the laser initiated detonations are well behaved. Cross sections of recovered cores such as that shown in Fig. 5 reveal reasonable good symmetry. By varying only the explosive density in a successful BN target design, straightforward scaling of the detonation pressure predicts adequate pressure for diamond formation. Even without spherically convergent pressure amplification, simple impedance match calculations indicate adequate pressures in the cast iron and low porosity copper-graphite targets.

It seems that there is a fundamental difference in the mechanisms responsible for shock production of wBN versus diamond. This has long been suggested by the predilection for gBN to form only the hexagonal wurtzite phase, whereas most graphite shots return the carbon in the cubic diamond phase. Static experiments[32] involving flash heating carbon under pressure suggest that recovery of diamond requires an annealing period. If the diamond transition in shocked carbon occurs by a similar mechanism, one might also expect that an annealing period is required. However, given the greatly reduced time scales of the shock experiments it seems reasonable that the annealing step might require higher temperatures but shorter durations. We suggest therefore that the failure to recover significant yields of diamond from small scale spherical targets may be due to insufficient time or temperature to anneal the product. It is interesting to note that the commercial shock synthesis of diamond is done on a scale three orders of magnitude larger than our experiments and produces yields in excess of 50%.[7]

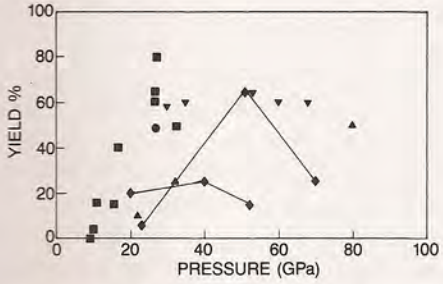

FIG. 7. Survey of wurtzite boron nitride yield as a function of shock pressure as reported by investigators using various shock processing arrangements (■ see Ref. 25; ▲ see Ref. 26 and 27; ▼ see Refs. 8 and 9; ● see Ref. 7; ♦ KMS fusion).

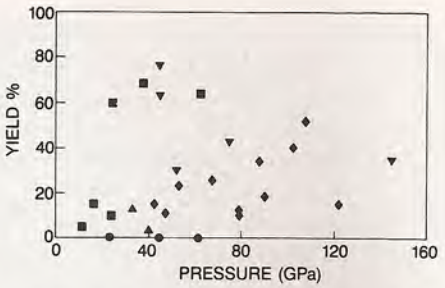

FIG. 8. Survey of diamond yield as a function of shock pressure as reported by investigators using various shock processing arrangements (■ see Ref. 28; ▲ see Ref. 22; ♦ see Ref. 6; ▼ see Ref. 7; ● KMS fusion).

VI. CONCLUSIONS

We have demonstrated that laser initiation can be used to ignite small scale spherically imploding detonations. A laser threshold for detonation has been measured. The characteristics of laser ignition indicate a thermal initiation mechanism occurring within a thin layer of the irradiated explosive. The laser initiated detonation is well behaved and has excellent symmetry at the millimeter scale of our targets.

Spherical implosions have been modeled by a one-dimensional hydrodynamic computer code. The modeling shows that the pressure increases with the spherical convergence of the imploding shock wave. Time-resolved and spatially resolved profiles of shock conditions in the payload have been calculated.

Recovery experiments provide evidence of spherical convergence. The formation of centrally located voids is attributed to tensile forces following reflection of the converged shock. Even stronger proof of spherical convergence is the recovery of wBN from the central zones of targets which could not have attained sufficient shock pressures without convergence.

Recovery experiments further demonstrated that wBN synthesis in small scale spherical geometry is consistent with other reports of shock synthesized wBN. On the other hand, some geometrical or scaling aspect of our spherical target design inhibits the recovery of shock synthesized diamond.

Small scale spherical shock processing may have a number of future applications. A system which could shock pro-

cess a 1-cm target each 10 s could meet a significant fraction of the world demand for ultrahard boron nitride. As a research tool the spherical processing technique has several attractive features, especially the high repetition rate and bench top capability. Other applications which we are pursuing presently include shock activated catalysts, shock driven organic chemistry, dynamic compaction of micron diamond powders,[33] and shock synthesis of new materials.

[1]P. S. DeCarli and J. C. Jamieson, Science **133**, 1821 (1961).
[2]N. L. Coleburn and J. W. Forbes, J. Chem. Phys. **48**, 555 (1968).
[3]W. H. Gust, Phys. Rev. B **22**, 4744 (1980).
[4]W. H. Gust and D. A. Young, Phys. Rev. B **15**, 5012 (1977).
[5]N. F. Bailey, in *Proceedings (Diamond in the 80's)*, A Technical Symposium sponsored by the Industrial Diamond Association of America, Inc., edited by G. S. Switzer (IDAA, Moorestown, NJ, 1980), p. 5.
[6]G. R. Cowan, N. J. Bruce, W. Dunnington, P. Wood, and A. H. Holtzman, U.S. Patent No. 3,401,019 (September 10, 1968).
[7]A. S. Balchan and G. R. Cowan, U.S. Patent No. 3,667,911 (June 6, 1972).
[8]A. Sawaoka, Ceram. Bull. **62**, 1379 (1983).
[9]M. Araki and Y. Kuroyama, Physica **139 & 140B**, 819 (1986).
[10]F. J. Mayer, U.S. Patent No. 4,522,742 (November 12, 1985).
[11]E. Lee, M. Finger, and W. Collins, Lawrence Livermore Laboratory Report No. UCID-16189, 1968 (unpublished).
[12]B. I. Bennett, J. D. Johnson, G. I. Kerley, and G. T. Rood, Los Alamos Scientific Laboratory Report No. LA-7130, 1978 (unpublished).
[13]C. L. Mader, *Numerical Modeling of Detonation* (University of California Press, Berkeley, CA, 1979).
[14]C. Y. Hsu, K. C. Hsu, L. E. Murr, and M. A. Meyers, in *Shock Waves and High Strain Rate Phenomena in Metals*, edited by M. A. Meyers and L. E. Murr (Plenum, New York, 1981), p. 433.
[15]W. Herrman, Sandia National Laboratory Report No. SC-RR-66-2678, 1968 (unpublished).
[16]R. A. Graham and D. M. Webb, in *Shock Waves in Condensed Matter*, edited by Y. M. Gupta (Plenum, New York, 1986), p. 831.
[17]F. R. Norwood, R. A. Graham, and A. Sawaoka, in *Shock Waves in Condensed Matter*, edited by Y. M. Gupta (Plenum, New York, 1986), p. 837.
[18]R. W. Perry and A. Kantrowitz, J. Appl. Phys. **22**, 878 (1951).
[19]A. A. Brish, I. A. Galeev, B. N. Zaitsev, E. A. Sbitnev, and L. V. Tatarintsev, Combust. Explos. Shock Waves **3**, 81 (1966).
[20]L. C. Yang and V. J. Menichelli, Appl. Phys. Lett. **19**, 473 (1971).
[21]V. B. Ioffe, A. V. Dolgolaptev, V. E. Aleksandrov, and A. B. Obraztsov, Combust. Explos. Shock Waves **21**, 316 (1985).
[22]A. I. Bykhalo, E. V. Zhuzhukalo, N. G. Koval'skii, A. N. Kolomiiskii, V. V. Korobov, A. D. Rozhkov, and A. I. Yudin, Combust. Explos. Shock Waves **21**, 481 (1985).
[23]F. J. Mayer, R. L. Maynard, D. L. Musinski, N. W. Schmerberg, M. R. Wixom, and R. F. Benjamin, in *Shock Waves in Condensed Matter*, edited by Y. M. Gupta (Plenum, New York, 1986), p. 547.
[24]C. E. Thomas, Appl. Opt. **14**, 1267 (1975).
[25]D. G. Morris, J. Appl. Phys. **51**, 2059 (1980).
[26]T. Soma, A. Sawaoka, and S. Saito, in *Proceedings of 4th International Conference on High Pressure*, Kyoto, 1974 (The Physico-Chemical Society of Japan, Tokyo, 1975), p. 446.
[27]J. M. Kruse, U.S. Patent No. 3,348,918 (October 24, 1967).
[28]A. N. Dremin, L. N. Breusov, T. V. Bavina, and S. V. Pershin, U.S. Patent No. 4,014,979 (March 29, 1977).
[29]T. Akashi (private communication).
[30]T. Akashi, A. Sawaoka, and R. A. Graham, in *Shock Waves in Condensed Matter*, edited by Y. M. Gupta (Plenum, New York, 1986), p. 821.
[31]N. Setaka, U. S. Patent No. 4,377,565 (March 22, 1983).
[32]F. P. Bundy and J. S. Kasper, J. Chem. Phys. **46**, 3437 (1967).
[33]D. K. Potter and T. J. Ahrens, Appl. Phys. Lett. **51**, 317 (1987).